PROCEEDINGS, 45th Workshop on Geothermal Reservoir Engineering
Stanford University, Stanford, California, February 10-12, 2020
SGP-TR-216

RLM-3D Multiphysics Inversion Modeling: De-Risking Resource Concept Models

Wolfgang Soyer, Randall Mackie, Stephen Hallinan, Federico Miorelli, Alice Pavesi, Stefano Garanzini

CGG Geoscience, Multi-Physics Imaging, Milan

wolfgang.soyer@cgg.com, randall.mackie@cgg.com, stephen.hallinan@cgg.com, federico.miorelli@cgg.com, alice.pavesi@cgg.com, stefano.garanzini@cgg.com

Keywords: Magnetotellurics, static distortion, multi-physics, 3D inversion, cooperative inversion, joint inversion, Sorik Marapi

ABSTRACT

The use of geophysics in delineating geothermal resources has made significant recent progress with the arrival of cost-efficient, complete earth 3D inversion modeling to augment the earlier adoption of 2D and 1D approximations. From recent studies at high enthalpy, volcanic-hosted geothermal prospects and production fields, we illustrate the RLM-3D inversion results from both single domain and joint inversion of magnetotellurics (MT), gravity and microearthquake (MEQ) datasets. The combined accuracy, parallelization and sophisticated regularization options enable fast inversion turnarounds over increasingly larger 3D meshes that include the critical MT and gravity data responses from both rugged topography, and the commonly adjacent sea water bodies. The regularization allows faults and other horizons, where present, to be represented correctly by sharp breaks in the otherwise relatively smooth 3D models. Galvanic distortion and true dipole lengths can also be included in the MT modeling, avoiding the ad hoc "corrections" applied previously as "MT static shifts".

RLM-3D includes solvers for MT, CSEM, gravity, gravity gradiometry, magnetics, and MEQ data (Vp, Vs, and event re-locations), and multi-discipline datasets are now routinely integrated with joint inversion workflows; this uses a cross-gradient technique promoting structural similarity between the inverted property volumes (resistivity, density, velocity, etc.). The same 3D technology also enables structural constraints from other sources, like geological, concept model scenarios under investigation, near surface dip and strike data to constrain shallow structural trends, fault surfaces, or seismic reflection volumes if available.

By accurately accounting for the real, 3D geological and topographic sources of geophysical data responses, we are now better equipped to integrate quantitatively all the available geophysical data to de-risk and finally update our working geothermal resource concept models.

1. INTRODUCTION

At volcanic-hosted, high enthalpy, geothermal fields the subsurface resistivity reflects primary lithology, secondary (hydrothermal) alteration grade and intensity, temperature, porosity and pore fluid salinity (Ussher et al., 2000; Cumming, 2009). Broadband magnetotellurics (MT) surveys, responding to the 3D resistivity distribution from a few tens of meters down to tens of kilometers depth, are therefore the most commonly employed geophysical technique during geothermal resource exploration. Ground gravity commonly accompanies MT as it responds to lateral density contrasts such as significant fault systems, vertically-oriented intrusives, and/or propylitic-altered density anomalies. During production and development phases, repeat precision gravity / levelling surveys and continuously recording MEQ arrays are increasingly deployed, mapping seismic event distributions, MEQ characteristics reflecting rock/fluid interactions, pressure/stress changes, fluid saturation changes, and production v. recharge balances.

Since the petrophysical relations between density, resistivity and velocity are far from straightforward in geothermal settings – varying across different lithology types – in joint inversion, we impose a structural similarity constraint between these properties using a 3D cross-gradient implementation. Following on from the cross-gradient joint inversion introduced by Gallardo and Meju (2003), we implemented a geothermal-oriented application to integrate MT, gravity and MEQ data, described in Soyer et al (2017, 2018).

We have also implemented fault surfaces as truly sharp discontinuities. The smoothness of regularization normally applied across the inversion cube can be interrupted with “tears” in the regularization process, defined along surfaces. To facilitate geologically-reasonable fault extents, we allow finite surface areas to be used, where the tear in the regularization also ends. A synthetic faulted system is illustrated, followed by inversion of measured MT and gravity data from Sorik Marapi, a geothermal field on the Great Sumatran fault.

Galvanic distortion in MT has concerned practitioners since the early days of the method, given its significant impact on depth modeling results. Tensor decompositions became popular in the 1980’s when most modeling was performed in 2D, and these methods provided insight into how small-scale structures distort otherwise 2D regional data, and enabled the assessment of the regional two-dimensionality of data sets (e.g. Groom and Bailey, 1989). The more recently developed phase tensors (Caldwell et al., 2004) are conceptually unaffected by electric galvanic distortion, and inversions using these impedance derived phase data do benefit from this quality (Tietze and Ritter, 2013) at the expense, however, of reduced absolute resistivity calibration. Soyer et al (2019) presented a joint inversion for 3D resistivity and site-specific distortion parameters, from MT impedances and vertical magnetic transfer function (Tz) data, if present, and the main results are illustrated here, along with considerations for finite MT electric dipole length.

2. MT DATA ISSUES AND 3D MODELING SOLUTIONS

2.1 MT sounding layout considerations

Finite or point dipole lengths: In most practical 2D and 3D modeling cases, the finite lengths of the electric dipoles are customarily ignored, as are the any lateral offsets of the sounding "center" with respect to model cell centers. In rugged topography, however, or over strongly varying conductive overburden thickness, we expect a difference between single point electric field solutions and explicit finite dipole calculations. The consideration of finite dipoles in modeling is in itself not new, and both Jones (1988) and Pellerin and Hohmann (1990) integrated fields along electrode positions to study the effect of small scale inhomogeneities on the averaged fields. Later we illustrated how topography also affects central loop TDEM soundings (Watts et al., 2013) showing the limitations for the use of TDEM for MT static shift remedy suggested by Pellerin and Hohmann. We were motivated by the desire to understand field distortions observed in voltage differences between electrodes, whether in the presence of detailed a priori information (LiDAR, drillhole data), differences between point and finite dipole solutions can and should be taken into account in 3D modeling, and how this is best addressed.

We generated a set of illustrative 3D models and have computed transfer functions from the calculated EM fields (Figure 1). The calculations are performed in two ways: the standard procedure of using fields interpolated to cell surface centers, and the integration of fields along the topographic surface between dipole end points, considering both horizontal and vertical field components.

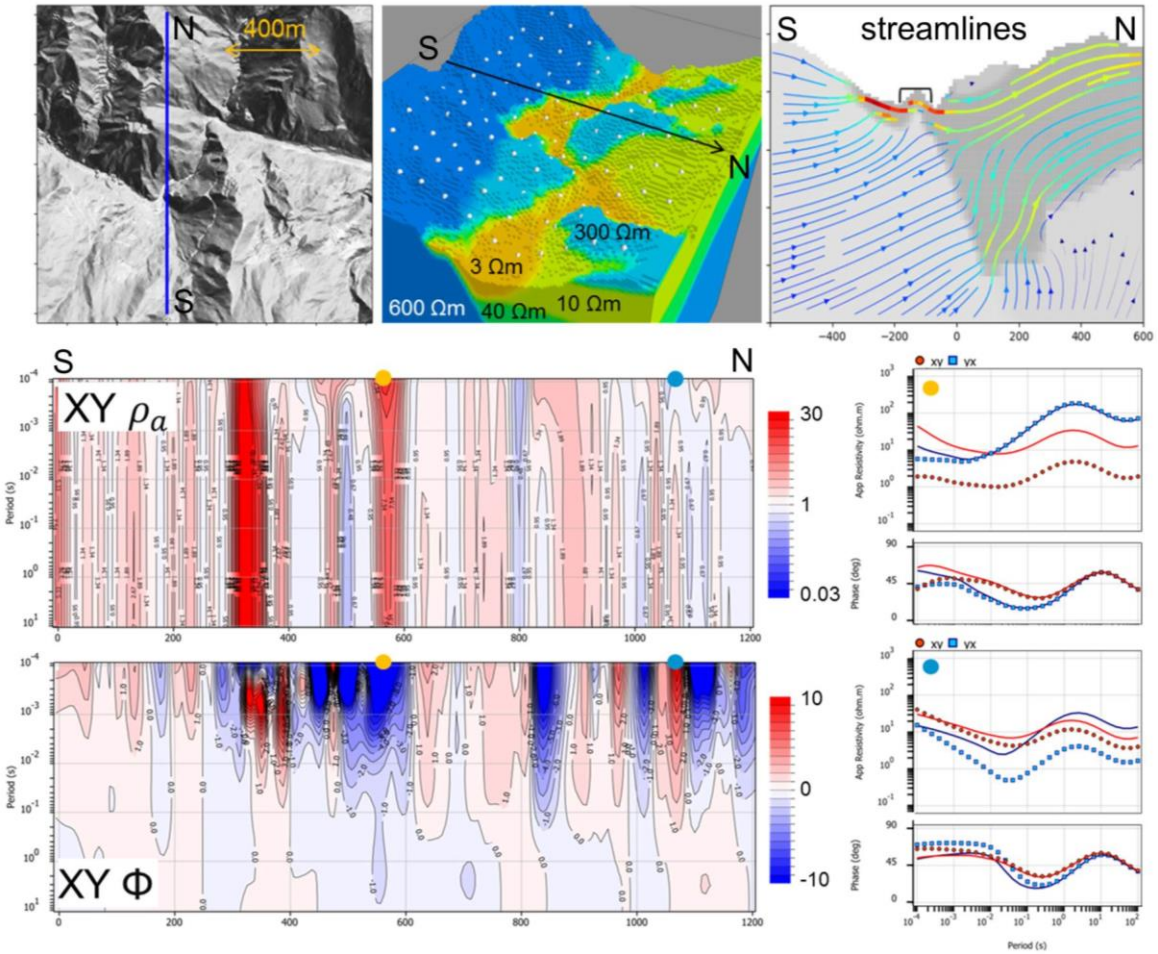

Figure 1 Example of steep topography from LiDAR (top left), and strong resistivity variation (rotated 3D model view, top center). Streamlines of currents (top right) at 3Hz along the marked line (polarization = Hy magnetic east, perpendicular to profile; resistivity in grey scale), with attraction of currents to the conductive valley sediments. Normalized pseudo-sections of finite dipole vs. point solutions show "static" effects in apparent resistivity, and phase differences, down to ~10Hz. 100m dipoles, model cells 12.5×12.5m laterally.

The electric field measurements (the "telluric" in MT) require grounded dipoles typically around 100m length to get high enough signal levels. While the dipoles are often extended across steep terrain and/or laterally variable near-surface resistivity, the finite length is treated as a point source by most modeling codes, and despite earlier investigations (e.g. Pellerin and Hohmann, 1990; Poll et al, 1989) the topic has received little attention recently. Soyer et al. (2019) looked at the effect of the dipole extent on measured data in several 3D model scenarios, including steep topography and strongly variable near-surface structure. The electric fields were integrated along the dipole lines in finely discretized models and divided by their length, and the resulting field estimates compared with solutions at the central surface cells of the dipoles. Effects are significant when the two electrodes are in different geo-electric environments – mainly steep topography and outcropping structure – and therefore different resistivity at each dipole electrode. Topography causes distortions that have a significant inductive (phase) component at frequencies down to 0.01Hz (Figure 1). Dipole effects from outcrops or faults may be stronger, especially when associated with current channeling, but are

essentially subsumed in the distortion model at low frequency, while for strong variation underneath *continuous* cover the effects are weaker.

MT soundings on slopes: An aspect of the MT measurement typically ignored is that it is done along the topographic *slope*, whereas modeling codes use the *horizontal* field component. This would require an amplitude correction of the inferred impedances, in order to scale down to the horizontal component. The differences between finite dipole solutions and modelled point solutions can largely – at frequencies <0.01-0.1Hz – be described by the galvanic distortion model for electric fields, as already pointed out by Pellerin and Hohmann (1990), and for 3D MT inversions, the more convenient use local solutions for electric fields is justified.

TMT soundings: In some MT surveys, not all channels of the data transfer functions are co-located, and magnetic channels are from a different location, either by survey design – e.g. for safety reasons – or due to sensor failures at certain MT setups. In these telluric-magnetotelluric (T-MT) situations, the true positioning of all channels is also taken into account in RLM-3D, where transfer functions calculated in the inversion process are computed from electric and magnetic fields at different locations.

2.2 Galvanic Distortion and Topography

MT electric field data are commonly subject to frequency-independent amplitude changes known as galvanic distortions (e.g. Jiracek 1990). These originate from small-scale structure that will not be successfully resolved in a 3D inversion, in a similar context to the measurement layout, as discussed above. Often with the original intention to provide a means to correct MT data for static distortions affecting electric field measurements (Pellerin and Hohmann, 1990) co-located central loop time domain (TDEM) may be available over a geothermal field, in particular for legacy data sets. These corrections can be essential for 1D layered earth inversions. However, in a 3D context, it also constitutes a tampering with observed data to address a phenomenon that is inherent in the MT method. Furthermore, TDEM data themselves are subject to effects from structural inhomogeneities and topography, and inversions of these data may lead to unrepresentative one-dimensional models (Watts et al., 2013). In 3D inversions, the requirement to account for galvanic effects in data input is more questionable, as the inversion can account for this remarkably well via inclusion of small-scale structure, while smoothing contains the impact on deeper structure. In fact, 3D inversion results from TDEM-corrected MT data using the above method typically compare well with those using original data. For contrasts of a somewhat larger scale, including topographic effects, it is more accurate to feed the original impedance tensors to the inversion.

For MT data with severe distortion effects, RLM-3D allows for a direct inversion for static distortion parameters (Soyer et al., 2018b, 2019). The galvanic distortion is represented by site-specific real-valued 2×2 matrices acting on the electric fields and therefore impedances across the entire frequency band; the distorted tensor Z_C can be written therefore as:

$$Z_C(f) = CZ(f) = \begin{pmatrix} C_{11} & C_{12} \\ C_{21} & C_{22} \end{pmatrix} \begin{pmatrix} Z_{xx}(f) & Z_{xy}(f) \\ Z_{yx}(f) & Z_{yy}(f) \end{pmatrix} \quad (1)$$

where Z is the 2×2 complex impedance tensor between the undistorted horizontal electric field and the magnetic field in frequency (f) domain, and C is the real-valued, frequency independent 2×2 distortion matrix.

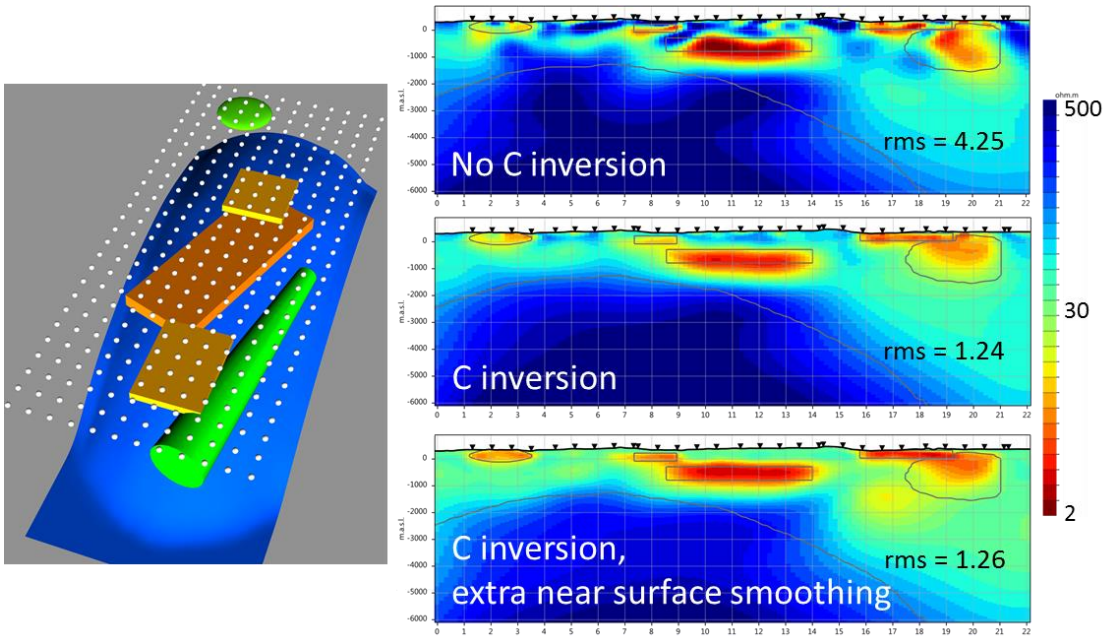

Figure 2 Synthetic 3D MT & Tz inversions. Left: input synthetic model ("N" top). Right: 3D inversion results along a "N-S" cross-section without inversion for distortion matrices (top), compared to results with C matrix inversion (center and bottom). Application of increased horizontal smoothing near surface (0-150m bsl, bottom section), apart from a smoother model, also leads to better recovery of input distortion matrices.

Inversion is simultaneous for 3D resistivity structure and distortion matrices, with a control parameter that suppresses deviations from the identity matrix, which represents the a priori condition of no distortion. With a very high value, distortions are suppressed and only significant when very strongly required by the data; with a very low value instead, the inversion is freer to introduce

impedance rotations and shifts in order to fit the data, rather than via resistivity structure. The distortion matrix estimation is therefore intrinsically linked with the structural smoothing constraint of the 3D inversion, and an intermediate choice will find the right balance between structure and distortion parameter estimations. Impedances and magnetic transfer functions were calculated from a synthetic model inspired by a geothermal setting; several shallow conductors (3-10Ωm) were embedded at different depth levels in a 50Ωm host, in turn sitting above a deeper, core resistor of 500Ωm. (Figure 1, details in Soyer et al 2019). 3D inversion for distortion matrices was also applied to the (real) Darajat MT data (Soyer et al. 2019) and show that considering C matrices does reduce shallow detail that is otherwise unresolved by the available MT data (Figure 3).

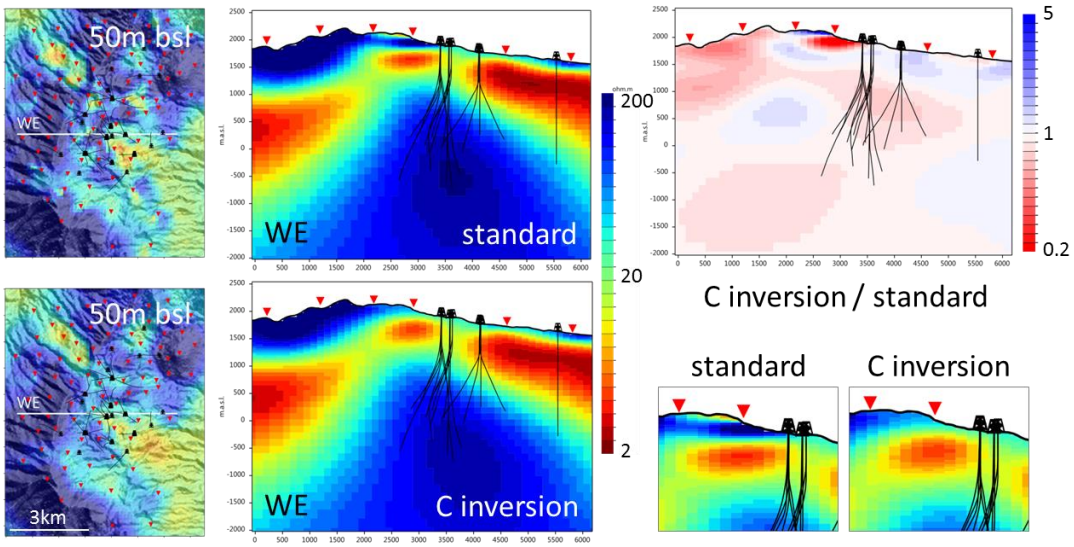

Figure 3 Darajat 3D MT inversions. Resistivity at 50m depth and along the WE profile, without (top) and with (bottom) inversion for distortion C matrices, and ratio of the two inversions (top right). Near surface resistivity is considerably smoother in the C inversion case. Zooming into the central shallow part (bottom right) shows the strongest changes.

In a further example (Figure 4), using the synthetic 3D geothermal field resistivity illustrated below in Figure 6, the calculated MT data were subjected to strong distortion using the parameter decomposition concept of Groom and Bailey (1989), adopting the same limits for uniformly distributed random numbers used by Soyer et al. (2018b) of ±0.5, ±45° and ±30° for anisotropy, twist and shear angles respectively. A logarithmically uniform distributed gain error was applied, within bounds of half an order of magnitude.

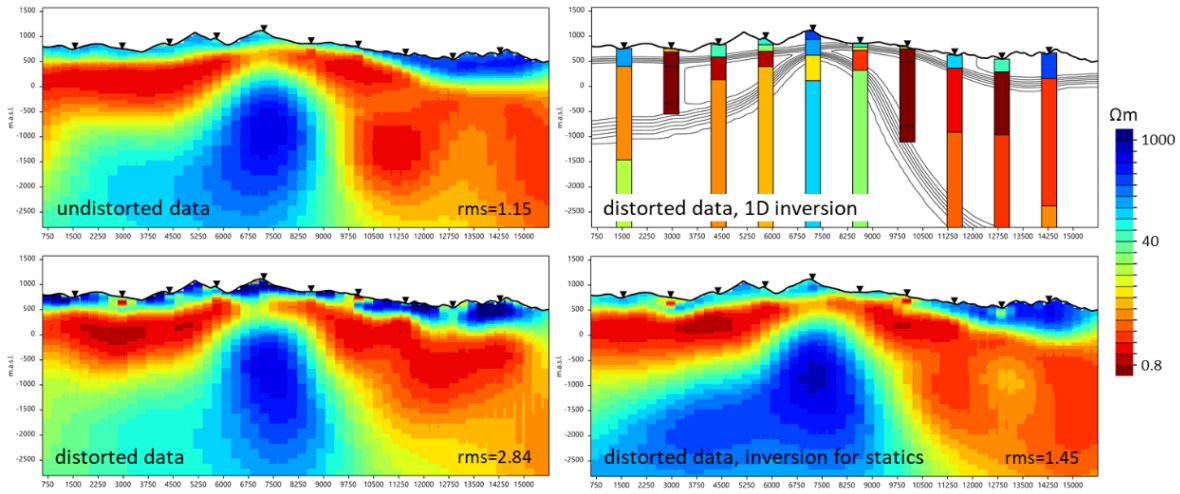

Figure 4 : Synthetic geothermal model (cf Figure 6) with effects of galvanic distortion on 1D, 3D MT inversions. VE 1.5.

MT single domain inversions of undistorted and distorted data are illustrated in Figure 4. Undistorted data are inverted to an accurate resistivity model – compare with contours shown on the 1D plot – and good data fit. To illustrate the strength of the distortion applied to the data set, 1D inversions of the tensor invariant determinant are overlain on the section as colored sticks, using the same resistivity color scale. These would indicate a wildly differing resistivity layering, and without 3D inversion, interpretation of these data would be very challenging. 3D inversion of the data in contrast provides fairly reliable results although data are fit only to an rms of ~2.8, and the main impact is a high shallow lateral resistivity variation. When inverting additionally for static distortion parameters, the shallow variability is attenuated, the deeper structure is more accurately modeled and the data fit improves considerably.

3. QUANTITATIVE INTEGRATION - BEYOND STRAIGHT JOINT INVERSION

Joint inversion is usually either cooperative or simultaneous. In a cooperative joint inversion, the result from one data type's inversion is integrated as a priori information into the inversion of the other type. In RLM-3D, this may be accomplished by using

structural cross-gradient inversion constrained by a previous inversion result; i.e. promote the inversion of data type 2 to be structurally similar with inversion results from data type 1. In the simultaneous joint inversion, data and model vectors of the inversion are the combination of the single type ones, and the inversion will update both properties at each iterations of the process. When further structural information is available, this can additionally be used; the two geophysical properties are linked via cross-gradients, and each or one of these is additionally cross-gradient linked to the reference model. Labelling the data misfit and model regularization terms Φ^{data} and Φ^{reg}, and cross-gradient terms between model properties Φ^{xg}, the objective function for a joint inversion takes the general form:

$$\Psi(\vec{\mathbf{m}}) = \sum_{j=1,2} \alpha_j \Phi_j^{data} + \sum_{i=a,b} \lambda_i \Phi_i^{reg} + \tau_{a,b}\, \Phi_{a,b}^{xg} \quad \left[+ \sum_{i=a,b} \tau_{i,ref} \Phi_{i,ref}^{xg} \right] \tag{2}$$

where $\vec{\mathbf{m}}$ is an ensemble of model properties (a, b). Indices j refer to different data types. Factors α, λ, and τ weight the contribution of the respective terms to the objective function (Commer and Newman, 2009). For the data weights, the ratio between the total numbers of data points of the two methods involved is used, but the weight can be adjusted.

3.1 Joint Inversion with reference to a structural concept model

Soyer et al (2018) presented the 3D joint inversion of MT, gravity and MEQ data from the Darajat steam field, referenced to the field's 3D porosity model gradients in order to quantitatively test the consistency of the geophysical data – at reasonable misfit – with the geological concept model represented by the porosity (Figure 5). While the joint inversion resistivity and density structures were indeed consistent with the porosity model, the tomographic velocity model inversions (Vp, Vs) were not, likely reflecting a stronger relationship to the reservoir fluid saturation as well as lithology and alteration.

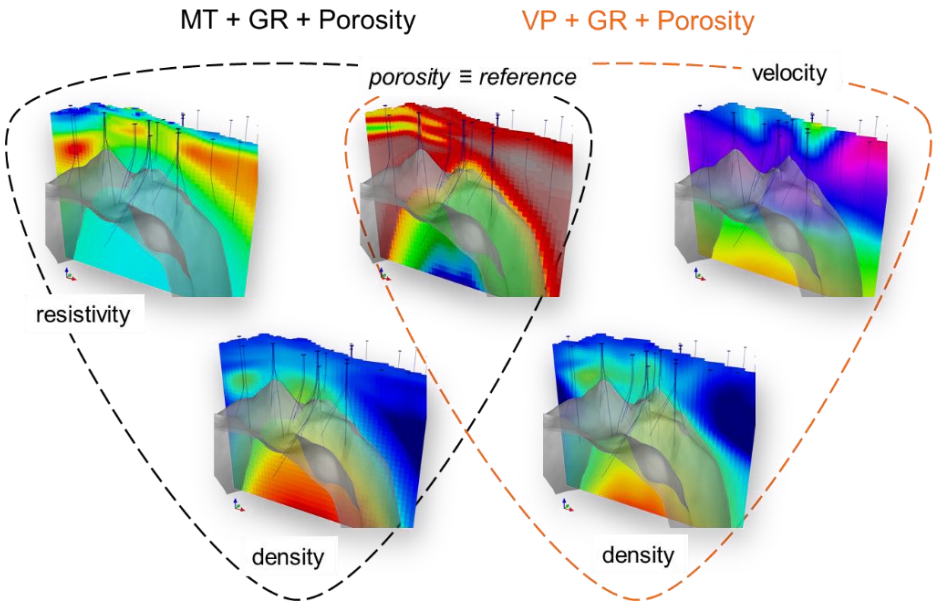

Figure 5 Joint inversions using cross-gradients to test consistency with the porosity volume structure; a proxy for the geological concept model. Inversion for resistivity and density (left), and velocity and density (right). In both cases, the porosity model (center top) was used as structural reference model. All cross-property linking was via cross-gradients. The transparent surface marks the estimated top of the andesite lava flows (drilled, extrapolated).

3.2 MT and gravity data responses over a geothermal field with graben

Here we present the cross-gradients as a way of integrating the different data types both in a cooperative and in a joint workflow while illustrating faults as tears in the inversion regularization, Firstly a generic, stand-alone synthetic study is examined, including distortion followed by joint analysis of measured MT and gravity data from the Sorik Marapi field (operated by KS Orka Renewables).

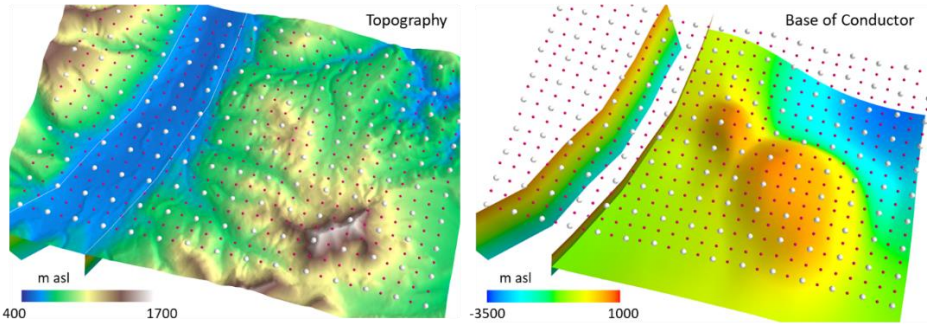

Figure 6 Structural setup for the synthetic study. Left: topography with fault outcrops and MT (white) and gravity (red) stations. Right: graben faults, and base of conductor topography under the simulated geothermal field.

Using real topography borrowed from a similar setting (Sumatra), a conceptual geothermal system was built with an up-doming, resistive and dense reservoir zone below a conductive and lower density clay alteration cap (Figure 4). The main graben fault tears extend to 3 km depth. The simulated geothermal field is adjacent to the graben structure, with typical three-layer scenario configured east of the graben and homogeneously resistive and denser "basement" rock to the west; the cross-section in Figure 7 (top row) illustrates the resistivity and density models.

All MT and gravity inversions started with homogeneous, half-space resistivity and density models. The single domain MT and gravity inversion models are shown in Figure 7 (left and right) with and without the use of regularization with tears at the faults (middle and bottom rows). While some detail at the base of conductor "cap" is missing, recovering the overall resistivity structure poses no major challenge to the MT inversion. As is the general case for unconstrained gravity inversions, however, while the lateral variations in density reflect the true case, the depth sensitivity is poor. Use of regularization with tears at the main faults results in sharper changes at the graben flanks – primarily to the west, and for gravity, which has a stronger integrated density change across the fault, also to the east. Structure recovery certainly improved *with* the tears.

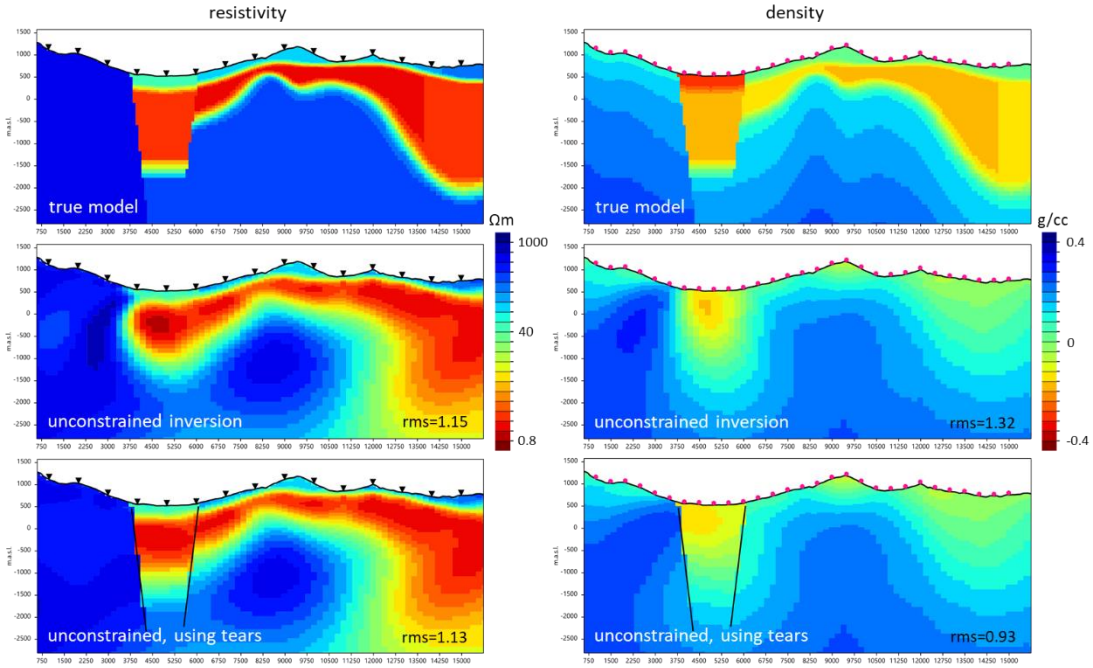

Figure 7 Synthetic modeling of MT (left) and gravity (right): true model structure (top); unconstrained single domain inversions without (center) and with (bottom) faults as regularization tear surfaces. Density scale is variation from 2.40 g/cc. V.E. = 1.5.

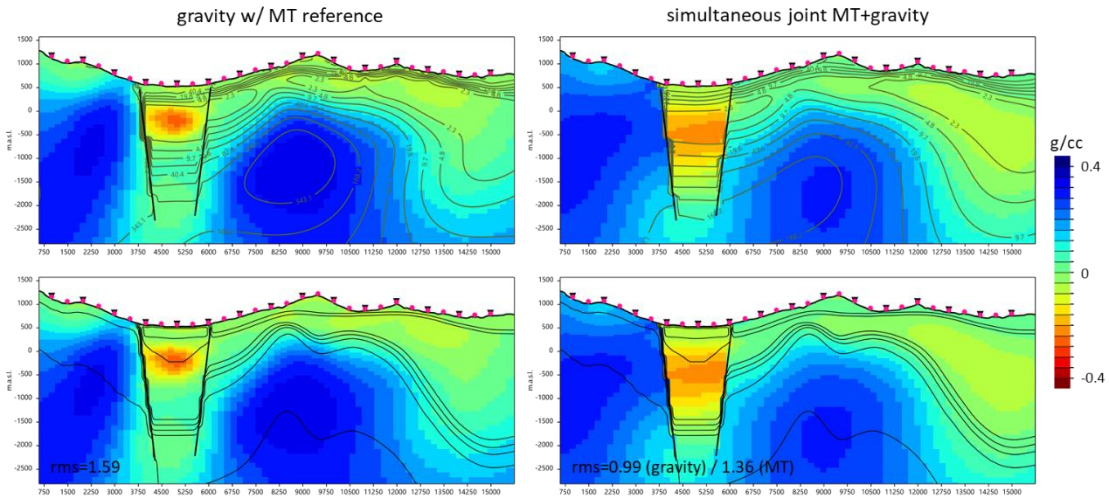

Figure 8 Cross-gradient gravity inversions including fault tears (all colour grids = density). Left: using the single domain MT inversion result as a structural reference. Right: simultaneous joint gravity+MT inversion. Top and Bottom compare the density inversions with line contours from the corresponding resistivity model (top) and the true density model (bottom). VE=1.5.

Cooperative (sequential) inversions and finally simultaneous joint inversions were then run. For the cooperative gravity inversions (Figure 8, left) the single domain MT inversion output (Figure 7 bottom left) was used as a fixed structural reference gradient model (cf. Soyer et al. 2018) during the gravity inversion. The simultaneous MT+gravity joint inversion (Figure 8 right) used a straightforward cross-gradient link between the MT and gravity inversion models, without a fixed reference model. The structure of the two density inversions (colour grids) is compared with the corresponding resistivity model (line contours, top row) and the true

density model (line contours, bottom row). In the central model area, the density structure recovery in both inversions has improved significantly over the single domain result. In the graben the low-density zone is now modelled as a focused anomaly, as in the MT inversion model. However, as in all the gravity inversions here, the near-surface low density zone is not resolved (Figure 7 top right).

3.3 Real Data Case: Sorik Marapi

The Sorik Marapi geothermal field (Sagala et al., 2016) is located within the low density, volcano-sedimentary sequence of the pull-apart graben structures along the main Sumatra fault, flanked by outcropping high density pre-Tertiary metamorphics. The Bouguer gravity reflects the graben structure, particularly the flanks where the strongest gravity gradients are observed (Figure 9). The fault delineations used in the inversion modeling are taken from geological maps where the faults outcrop, and from the gravity gradient maxima where not. Steep, normal fault dips of 80° were assumed, extending to 3km depth. These finite length tears in the regularization were tested in a suite of inversion runs (Figure 10). Bouguer gravity data were assigned a 0.3mGal error, and relative density changes were inverted with respect to the reduction density 2.40g/cc. MT data were inverted within the frequency band of 0.0016-2500Hz, with five frequencies per decade. All resistivity and density inversion starting models were homogeneous half-spaces.

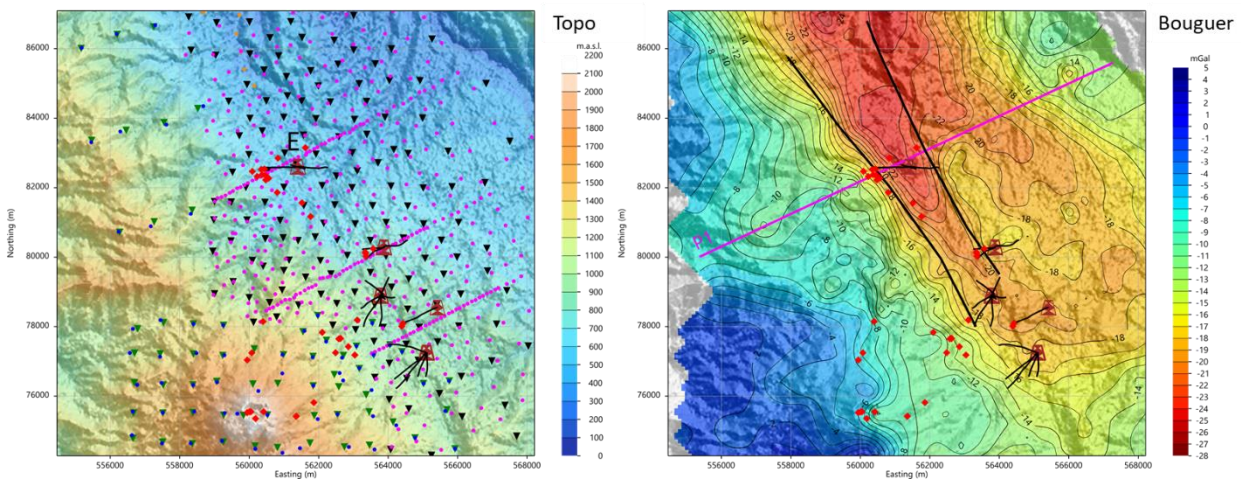

Figure 9 Left: Sorik Marapi topography, showing SM volcano near southern margin, with MT (triangles), gravity (points), hot springs and fumaroles (red) and well traces. Right: Complete Bouguer gravity anomaly at 2.40g/cc, with reverse color scale (as resistivity). The two black NW-SE lines mark faults from surface geological mapping and tracing the gravity gradient maxima.

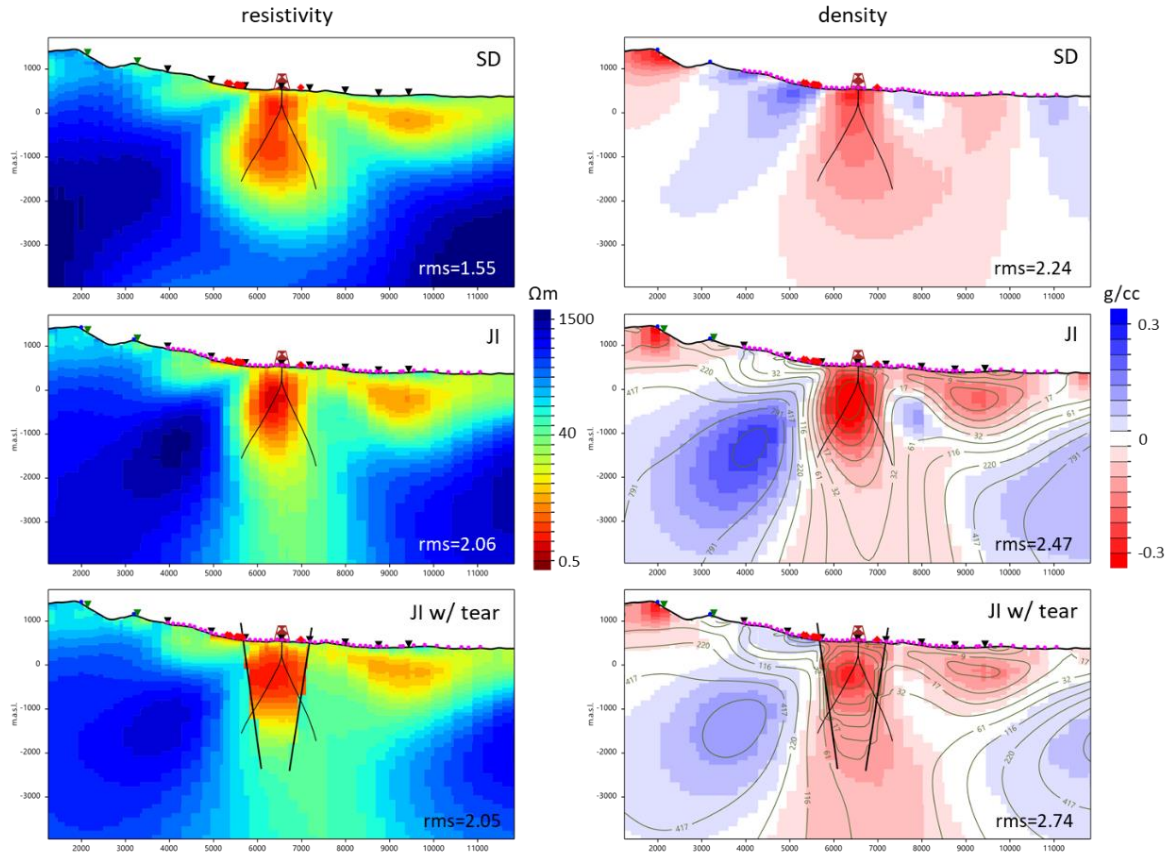

Figure 10 Dip section through pad E well traces of MT (left) and gravity (right) inversions; single inversions (top) with cross-gradient joint inversions center (no faults) and bottom (with faults). VE=1.

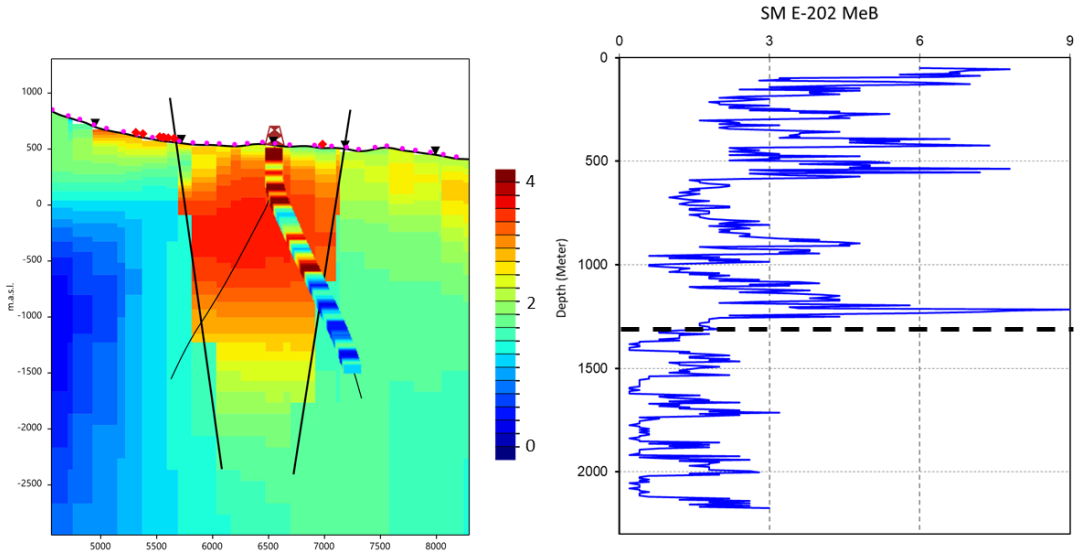

Figure 11 Left: resistivity from joint gravity-MT inversion + fault tears (grid color scale as Error! Reference source not found.**) with MeB summary overlain along the well trace. The MeB color bar (center) refers to the smoothed MeB readings. Right: MeB log with modeled fault location projected at the black dash.**

As in the synthetic example, and typical for MT and gravity data types, the MT inversions are more robust than the gravity ones, with little difference between single and joint domain outputs within the depths of interest, while gravity inversions improved considerably with the inclusion of shallow depth information from the MT models (Figure 10). The use of regularization with tears at the faults results in sharp boundaries specifically at the western limit of the graben, and accordingly less artifacts (lower overshoot to higher resistivity) from the smoothing. The fault intersections along the two pad E wells were unknown during the inversion modeling exercise. Methylene blue data (MeB, sensitive to smectite) from one well became available after the inversions. These are overlain on the joint gravity+MT inversion with tears (Figure 11), showing excellent MeB correlation with the resistivity break at the modeled fault location.

5. CONCLUSIONS

Through integrated modeling of multiple geophysical data types over geothermal fields, we ultimately aim at deriving a geologically reliable multi-property 3D model that consistently explains the observations of each geophysical dataset. Since analytic, petrophysical relations between density and resistivity are far from straightforward in geothermal settings, varying across different lithology types, we impose a structural similarity constraint between them using a cross-gradient implementation in our inversion engine RLM-3D. Inclusion of a priori information, if available – like density logs from wells, or a porosity volume from a geophysical concept model – allows further constraints in the RLM-3D inversions. The latter approach can also be used to test different scenarios or concept models, finding those that are consistently in agreement with the observed data available.

Considering cooperative vs joint inversion of MT and gravity data, while MT results were largely similar for both single and joint domain inversions, the gravity inversions – with inherently weaker depth sensitivity than MT – benefited significantly from the integration, in both cooperative and joint workflows. In the synthetic example, the joint approach yielded better results.

We have implemented 3D faults as discontinuity surfaces, of finite extent, in the RLM-3D inversion regularization, and used the scheme during both single domain and cross-gradient joint inversions of geothermal MT and gravity datasets, firstly for a synthetic case, and then for the Sorik Marapi field data. Through integrated, quantitative modeling of multiple geophysical data types over geothermal fields, now including faults as sharp discontinuities, we facilitate geologically and structurally reliable multi-property 3D earth models that consistently explain the observations of different geophysical datasets.

Regarding geologically-related MT data "distortions", RLM-3D includes a robust means to deal with rugged topography and galvanic distortion effects, avoiding the pitfalls inherent in using "corrections" based on TDEM data that also enjoy topographic and local structure distortions. Looking at other data distortions from point vs finite electric dipole considerations in 2D and 3D modeling, we conclude that the difference between single cell and finite dipole calculations is particularly strong for outcropping structure, as expected. For the case of a continuous overburden, effects from dipole extent are weaker, in particular over the thicker parts of the overburden interval. In complex 3D settings, the incorrect inclusion of the finite dipole length leads to distorted modeling and structure interpretation. To include this concept into a 3D inversion procedure, the explicit consideration of finite dipoles would need to be considered also during the calculation of adjoint fields and sensitivities.

ACKNOWLEDGMENTS

The authors would like to express their gratitude to KS Orka and Star Energy for the permission to publish the results from the 3D inversion modeling of the Sorik Merapi and Darajat geophysics data respectfully. We also thank our CGG colleague Carsten Scholl for valuable advice on the distortion modeling.

REFERENCES

Caldwell, T.G., Bibby, H.M. and Brown, C.: The magnetotelluric phase tensor, Geophys. J. Int. (2004) 158, 457–469

Commer, M., and Newman, G.A.: Three-dimensional Controlled-Source Electromagnetic and Magnetotelluric Joint Inversion, Geophysical Journal International, 178, (2009), 1305-1316.

Cumming, W.: Geothermal Resource Conceptual Models Using Surface Exploration Data, Proceedings, *34th Workshop on Geothermal Reservoir Engineering*, Stanford University, Stanford, CA (2009).

Gallardo, L.A., and Meju, M.A.: Characterization of Heterogeneous Near-Surface Materials by Joint 2D Inversion of DC Resistivity and Seismic Data, *Geophysical Research Letters*, **30**(13), (2003), 1658.

Groom, R.W., and Bailey, R.C.: Decomposition of Magnetotelluric Impedance Tensors in the Presence of Local three dimensional Galvanic Distortion, *Journal of Geophysical Research*, **94**, (1989), 913–1925.

Jiracek, G.R.: Near-surface and Topographic Distortions in Electromagnetic Induction, *Surveys in Geophysics*, **11**(2-3), (1990), 163-203.

Jones, A.G.: Static Shift of Magnetotelluric Data and its Removal in a Sedimentary Basin Environment, *Geophysics*, **53**(7), (1988), 967-978.

Pellerin, L., and Hohmann, G.W.: Transient Electromagnetic Inversion: A Remedy for Magnetotelluric Static Shifts, *Geophysics*, **55**(9), (1990), 1242-1250.

Sagala, B.D., Chandra, V.R., and Purba, D.P.: Conceptual Model of Sorik Marapi Geothermal System based on 3-G Data Interpretation, *ITB International Geothermal Workshop*, Bandung, Indonesia (2016).

Soyer, W., Mackie, R.L., Hallinan, S., Pavesi, A., Nordquist, G., Suminar, A., Intani, R., and Nelson, C.: Multi-Physics Imaging of the Darajat Field, *Geothermal Research Council Annual Meeting*, Salt Lake City, UT, *Transactions*, 41, (2017).

Soyer, W., Mackie, R.L., Hallinan, S., Pavesi, A., Nordquist, G., Suminar, A., Intani, R. and Nelson, C.: Geologically-consistent Multiphysics Imaging of the Darajat Geothermal Steam Field, *First Break*, **36**(6), (2018a), 77-83.

Soyer, W., Mackie, R.L. and Miorelli, F.: Optimizing the Estimation of Distortion Parameters in Magnetotelluric 3D Inversion, *80th EAGE Conference and Exhibition*, Copenhagen, Denmark (2018b).

Soyer, W., Mackie, R.L., and Miorelli, F.: Comparative Analysis and Joint Inversion of MT and ZTEM Data, *AEM, 7th International Workshop on Airborne Electromagnetics*, Kolding, Denmark (2018c).

Soyer, W., Miorelli, F. and Mackie, R.L.: Considering True Layout Geometry in Magnetotelluric Modeling *Extended Abstract*, 24th EM Induction Workshop, Helsingør, Denmark (2018d).

Soyer, W., Miorelli, F. and Mackie, R.L.: On the Effects of Finite Dipoles in 3-D Magnetotelluric Modeling, *81st EAGE Conference and Exhibition*, London, UK (2019).

Tietze, K., and O. Ritter: 3D Magnetotelluric Inversion in Practice - The Electrical Conductivity Structure of the San Andreas Fault in Central California, *Geophysical Journal International*, 195(1), (2013), 130- 147.

Ussher, G., Harvey, C., Johnstone, R., and Anderson, E.: Understanding the Resistivities Observed in Geothermal Systems, *Proceedings, World Geothermal Congress*, Kyushu-Tohoku, Japan (2000).

Wannamaker, P.E., Stodt, J.A., and Rijo, L.: Two-dimensional Topographic Responses in Magnetotelluric Responses in Magnetotellurics Modeled Using Finite Elements, *Geophysics*, **51**(11), (1986), 2131-2144.

Watts, M.D., Mackie, R.L., Scholl, C. and Hallinan S.: Limitations of MT Static Shift Corrections Using Time-Domain EM Data, *Extended Abstracts*, SEG Annual Meeting, Houston, TX (2013).